Noise suppression of transport through double quantum dots by feedback control

Jiahao Xu,[1] Shikuan Wang,[2] Jiawei Wu,[1] Yiying Yan,[1] Jing Hu,[1] Georg Engelhardt,[3,4,5] and JunYan Luo[1,*]

[1]*Department of Physics, Zhejiang University of Science and Technology, Hangzhou 310023, China*

[2]*Department of Physics, Hangzhou Dianzi University, Hangzhou 310018, China*

[3]*Shenzhen Institute for Quantum Science and Engineering, Southern University of Science and Technology, Shenzhen 518055, China*

[4]*International Quantum Academy, Shenzhen 518048, China*

[5]*Guangdong Provincial Key Laboratory of Quantum Science and Engineering, Southern University of Science and Technology, Shenzhen, 518055, China*

(Received 4 November 2022; revised 3 February 2023; accepted 9 February 2023; published 7 March 2023)

A controllable low noise current lies at the heart of high-precision measurements in quantum transport and metrology. While the previous research dealt with the suppression of noise in transport through a tunneling junction or a single quantum dot (QD) device, the present work investigates noise inhibition of a double quantum dot (DQD) transport system based on closed-loop feedback control. The unique advantage of a DQD device is that bidirectional transport at low bias can be measured by a nearby quantum point contact. However, the continuous monitoring of the DQD states inevitably leads to a measurement-induced dephasing. To appropriately characterize its transport properties in the presence of feedback action, we here develop a numerical method dubbed auxiliary density matrix approach, motivated by the hierarchical expansion of the moment-generating function in the hierarchy equations of motion [J. Cerrillo *et al.*, Phys. Rev. B **94**, 214308 (2016)]. This generic method has no restriction on the system structure and parameters and is able to evaluate the feedback current cumulants to an arbitrary order. It is revealed that the feedback control of the tunnel coupling between the two dots is the most effective to suppress the noise under various tunnel coupling configurations. The influence of interdot Coulomb interaction, measurement-induced dephasing, and finite time delay on feedback is also analyzed in detail.

DOI: 10.1103/PhysRevB.107.125113

I. INTRODUCTION

Quantum fluctuations in nonequilibrium transport through nanostructures are a fundamental physical phenomenon due to the quantization of the electron charge [1–3]. In particular, the state-of-the-art real-time detection technology has experimentally allowed a systematic characterization of temporal correlations between individual electron transfers [4–9]. Noise suppression and enhancement both have been observed in single-electron devices. Normally, the Pauli exclusion principle inhibits the noise below the classical Poisson value [10–14]. Yet, it is revealed that super-Poissonian noise can appear, for instance, in the cotunneling regime [15–17] or in the presence of a dynamical channel blockade mechanism [18–23]. These investigations have demonstrated that noise is a sensitive diagnostic tool to probe intriguing correlations between carriers. However, it is also of great importance to shed light on how to manipulate these correlations to achieve a controllable low noise current, paving thus the way for high-precision measurements in quantum transport and quantum metrology.

Quantum feedback control is a promising candidate to effectively impose additional correlations between charge transfers. Yet, its application for noise suppression in quantum transport has only been proposed recently in a tunneling junction or single QD on the level of single electrons [24–26]. Remarkably, strong suppression of charge fluctuations has been achieved in experiment for transport through a single QD based on a closed-loop feedback scheme, where the information of real-time individual electron tunneling measured by a nearby quantum point contact (QPC) is used to appropriately adjust the tunneling rates between the single QD and the electrodes [27].

In comparison with a single QD device, a "nonlocal" DQD system manifests more pronounced and rich physics and exhibits a number of unique effects [28,29], serving thus not only as an ideal testbed to investigate fundamental principles in quantum mechanics but also as a promising candidate for quantum information processing [30–33]. It has been demonstrated that the transport characteristics in a DQD depends sensitively on a number of its unique internal and coupling parameters, such as many-body effects [34–39], quantum coherence [39–42], system-bath coupling [42–46], detuning [47–51], and interdot tunnel coupling [52–55]. Essentially, different from a single QD where only unidirectional transport counting statistics can be measured under strongly nonequilibrium conditions, a DQD device has the intriguing advantage to count bidirectional single electron transfers in a nearly equilibrium condition [56]. Yet, this relies on a QPC detector which, on one hand, extracts the DQD information in a continuous manner and, on the other hand, alters the

*jyluo@zust.edu.cn

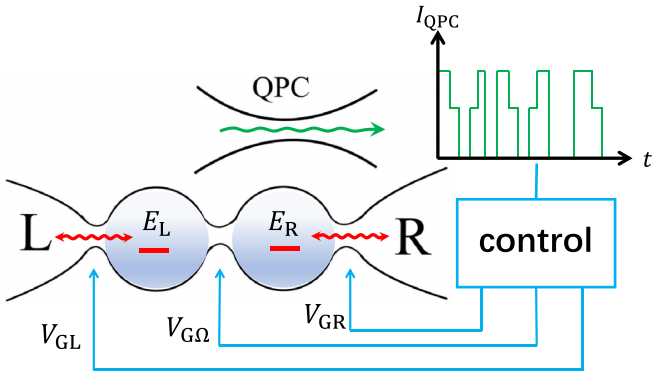

FIG. 1. Schematics of closed-loop feedback control of transport through a DQD tunnel coupled to the left and right electrodes. A nearby QPC is electrostatically coupled to the two dots in an asymmetrical way such that the jumps of the QPC current $I_{\rm QPC}$ (top right) reveal the bidirectional electron tunneling through the DQD. The discrepancy between the measured and target currents through the DQD is then used to feedback control the gate voltages $V_{\rm GL}$, $V_{\rm GR}$, and $V_{\rm G\Omega}$, which corresponds to an appropriate modification of the tunnel couplings $\Gamma_{\rm L}$, $\Gamma_{\rm R}$, and Ω, to regulate the discrepancy of the DQD current in the next time interval.

remaining uncertainty in the DQD system, leading inevitably to a dephasing mechanism in the measured system. This brings not only additional freedom but also poses great challenges to feedback control of transport through a DQD system. It is therefore appealing to describe feedback transport characteristics with full accounting for these factors and investigate essentially how effective the feedback is to stabilize low noise currents through DQD devices.

Due to the feedback action, the equation of motion for the moment-generating function becomes a partial differential equation, that can be solved only in special cases. Motivated by the hierarchical expansion of the moment-generating function in the hierarchy equations of motion [57], our work develops a numerical method dubbed "auxiliary density matrix approach" that keeps track of the counting statistics in the presence of feedback action. This generic method has no restriction on the system structure and parameters. It maps the first-oder partial differential equation to a set of coupled ordinary differential equation, that can be conveniently numerically integrated.

The system under study is schematically shown in Fig. 1, where a nearby QPC is electrostatically coupled to the two dots in an asymmetrical way such that the jumps of the QPC current $I_{\rm QPC}$ reveal the real-time information of the stochastic electron tunneling through the DQD. The discrepancy between the measured and target currents through the DQD is then used to feedback control the gate voltages $V_{\rm GL}$, $V_{\rm GR}$, and $V_{\rm G\Omega}$, which corresponds to an appropriate modification of the tunnel couplings $\Gamma_{\rm L}$, $\Gamma_{\rm R}$, and Ω in such a way that the tunneling process is adjusted to compensate the discrepancy of the DQD current in the next time interval. Our investigation demonstrates unambiguously that the feedback scheme works in both high and low bias limits. In particular, it is revealed that the feedback control of the tunnel coupling between the two dots is the most effective to suppress the noise under various feedback control parameters. Furthermore, we also analyze how the measurement-induced dephasing, interdot charging energy, and finite time delay influence the feedback performance.

The rest of the paper is organized as follows. We start with a description of the DQD transport system and its full counting statistics (FCS) in Sec. II, which is then followed in Sec. III by the introduction of the feedback scheme and establishment of the auxiliary density matrix approach for feedback transport properties. Section IV is devoted to a detailed investigation on the effectiveness of feedback control of transport through a DQD under various conditions. Finally, we summarize the work in Sec. V.

II. MODEL SYSTEM AND FULL COUNTING STATISTICS

The DQD transport system is schematically shown in Fig. 1, where the two dots, contacted in series, are tunnel coupled to the left and right electrodes. The Hamiltonian of the whole system reads [28,56,58–60]

$$H = H_{\rm S} + H_{\rm B} + H_{\rm I}, \tag{1}$$

where $H_{\rm S}$ denotes the Hamoltonian of the DQD. In the dot state representation $|0\rangle$, $|{\rm L}\rangle$, $|{\rm R}\rangle$, $|{\rm D}\rangle$, standing for no electrons, one electron in the left dot, one in the right dot, and one in each dot, respectively, the DQD Hamiltonian can be expressed as

$$H_{\rm S} = \sum_{\ell} E_\ell d_\ell^\dagger d_\ell + \Omega(d_{\rm L}^\dagger d_{\rm R} + d_{\rm R}^\dagger d_{\rm L}) + U d_{\rm L}^\dagger d_{\rm L} d_{\rm R}^\dagger d_{\rm R}, \tag{2}$$

where d_ℓ ($d_\ell^\dagger$) is the annihilation (creation) operator for an electron in the left ($\ell = {\rm L}$) or right ($\ell = {\rm R}$) dot, and Ω is the interdot tunnel coupling strength. $E_{\rm L/R}$ is the single energy level in the left ($\ell = {\rm L}$) or right ($\ell = {\rm R}$) dot within the bias window. One may parametrize the single levels by their average energy $\bar{E} = (E_{\rm L} + E_{\rm R})/2$ and their difference $\Delta E = E_{\rm L} - E_{\rm R}$, such that $E_{\rm L/R} = \bar{E} \pm \frac{1}{2}\Delta E$. The interdot Coulomb charging energy U is associated with the energy cost for simultaneous occupation of one electron in each dot. The intradot (on-site) Coulomb interactions are assumed to be infinite such that the double occupation of each dot is energetically not allowed. The electron spin label is suppressed here and in the following, since only charge states play a role. This depiction has been shown to be useful for modeling charge-related properties in individual DQD devices [61,62].

The left and right electrodes are modeled as reservoirs of noninteracting electrons

$$H_{\rm B} = \sum_{\ell={\rm L,R}} \sum_k \varepsilon_{\ell k} c_{\ell k}^\dagger c_{\ell k}, \tag{3}$$

where $c_{\ell k}$ ($c_{\ell k}^\dagger$) is the annihilation (creation) operator for an electron with momentum k in the left ($\ell = {\rm L}$) or right ($\ell = {\rm R}$) electrode. The electrodes are assumed to be in local equilibrium and characterized by the Fermi distribution $f_\ell(\omega) = \{1 + e^{(\omega-\mu_\ell)/k_{\rm B}T_\ell}\}^{-1}$, where T_ℓ and μ_ℓ are respectively the temperature and chemical potential in electrode ℓ. This spinless model could be motivated by a large magnetic field that leads

to complete spin polarization in the leads, such that only one spin would need to be considered, or alternatively by orbitals where all tunneling processes are completely symmetric in the electronic spin, such that it may be omitted from our considerations.

The tunnel coupling between the DQD and the electrodes is described by the Hamiltonian

$$H_{\rm I} = \sum_{\ell={\rm L,R}} \sum_{k} (t_{\ell k} c_{\ell k} d_{\ell}^{\dagger} + {\rm H.c.}), \tag{4}$$

where $t_{\ell k}$ is the tunneling amplitude between the DQD and electrode ℓ. The corresponding tunnel coupling strength is characterized by the intrinsic linewidth $\Gamma_\ell(\omega) = 2\pi \sum_k |t_{\ell k}|^2 \delta(\omega - \varepsilon_{\ell k})$. In the usual wide-band limit, it becomes energy independent $\Gamma_\ell(\omega) = \Gamma_\ell$. Throughout this work, we set $e = \hbar = 1$.

Electron tunneling through the DQD is measured by a nearby QPC, which is modeled as a tunneling junction whose conductance is susceptible to changes in the surrounding electrostatic environment (the occupation of the DQD). The asymmetrical electrostatic coupling between DQD and QPC results in different QPC currents, i.e., $I^{\rm L}_{\rm QPC}$ ($I^{\rm R}_{\rm QPC}$) when the left (right) dot is occupied. It is due to this mechanism that the QPC is able to continuously measure the quantum state of the DQD and thus deduce electron tunneling through the DQD in both forward and reverse directions. This however gives rises to an additional measurement-induced dephasing of the DQD system [63,64]

$$\gamma_d = \tfrac{1}{2}\big(\sqrt{I^{\rm L}_{\rm QPC}} - \sqrt{I^{\rm R}_{\rm QPC}}\big)^2. \tag{5}$$

This is a striking difference in comparison with the charge transport though single QD devices.

The stochastic nature of transport is characterized by the probability distribution $P(N,t) = {\rm tr}\{\rho^{(N)}(t)\}$ for the number N of electrons transferred through the DQD in the time interval $[0,t]$, where $\rho^{(N)}(t)$ is the reduced density matrix conditioned on the transfered electrons satisfying $\rho(t) = \sum_N \rho^{(N)}(t)$ [65]. A powerful tool to characterize this probability distribution is the FCS [2,3], that encodes the statistical information in terms of the cumulant generating function (CGF) $\mathcal{F}(\chi,t)$ defined by

$$e^{\mathcal{F}(\chi,t)} = \sum_N P(N,t) e^{-iN\chi} = {\rm tr}\{\rho(\chi,t)\}. \tag{6}$$

We have here introduced the χ-dependent reduced density matrix $\rho(\chi,t) = \sum_N \rho^{(N)}(t) e^{iN\chi}$, where χ is the counting field associated with the number of tunneled electrons. Under the second-order Born-Markov approximation, $\rho(\chi,t)$ satisfies the following χ-dependent quantum master equation [2,3]

$$\dot{\rho}(\chi,t) = \mathcal{L}(\chi)\rho(\chi,t). \tag{7a}$$

In the dot states representation of the DQD, the reduced density matrix can be expressed as a column vector $\rho \equiv (\rho_{00}, \rho_{\rm LL}, \rho_{\rm RR}, \rho_{\rm DD}, {\rm Re}[\rho_{\rm LR}], {\rm Im}[\rho_{\rm LR}])^{\rm T}$, where $\rho_{aa} \equiv \langle a|\rho|a\rangle$ denotes the probability of the DQD in the state $|a\rangle$ ($a = 0, {\rm L}, {\rm R}, {\rm D}$), $\rho_{\rm LR} \equiv \langle {\rm L}|\rho|{\rm R}\rangle$ stands for the so-called "quantum coherence." The other nondiagonal elements between states of different electron numbers, such as $\rho_{0\rm L}$, $\rho_{\rm RD}$, etc., are dynamically decoupled and thus not included. In this case, $\mathcal{L}(\chi)$ is explicitly given by

$$\mathcal{L}(\chi) = \begin{pmatrix}
-\sum_{\ell={\rm L,R}} \Gamma_\ell^+ & \Gamma_{\rm L}^- & e^{i\chi}\Gamma_{\rm R}^- & 0 & 0 & 0 \\
\Gamma_{\rm L}^+ & -\Gamma_{\rm L}^- - \tilde{\Gamma}_{\rm R}^+ & 0 & e^{i\chi}\tilde{\Gamma}_{\rm R}^- & 0 & 2\Omega \\
e^{-i\chi}\Gamma_{\rm R}^+ & 0 & -\Gamma_{\rm R}^- - \tilde{\Gamma}_{\rm L}^+ & \tilde{\Gamma}_{\rm L}^- & 0 & -2\Omega \\
0 & e^{-i\chi}\tilde{\Gamma}_{\rm R}^+ & \tilde{\Gamma}_{\rm L}^+ & -\sum_{\ell={\rm L,R}} \tilde{\Gamma}_\ell^- & 0 & 0 \\
0 & 0 & 0 & 0 & -\frac{1}{2}\sum_{\ell={\rm L,R}} (\Gamma_\ell^- + \tilde{\Gamma}_\ell^+) - \gamma_d & -\Delta E \\
0 & -\Omega & \Omega & 0 & \Delta E & -\frac{1}{2}\sum_{\ell={\rm L,R}} (\Gamma_\ell^- + \tilde{\Gamma}_\ell^+) - \gamma_d
\end{pmatrix}, \tag{7b}$$

where the tunneling rates are defined as $\Gamma_\ell^{\pm} = \Gamma_\ell f_\ell^{(\pm)}(\bar{E})$ and $\tilde{\Gamma}_\ell^{\pm} = \Gamma_\ell f_\ell^{(\pm)}(\bar{E} + U)$, with the Fermi function $f_\ell^{(+)}(\omega) = f_\ell(\omega)$ and $f_\ell^{(-)}(\omega) = 1 - f_\ell^{(+)}(\omega)$. Here, we are interested in the regime $\Delta \ll k_{\rm B}T$ ($\Delta = \sqrt{\Delta E^2 + 4\Omega^2}$ being the eigenenergy separation), where the external coupling strongly modifies the internal dynamics [44,58,62,65], the level separation is thus smeared by the temperature, and only the excitation energies $\bar{E}$ and $\bar{E} + U$ enter the Fermi functions. The tunnel coupling induced energy renormalization, or the so-called Lamb shift due to system-bath coupling [43,44,66] has been included in ΔE. The counting of electron tunneling events in forward and reverse directions is implied by the sign of the exponential in Eq. (7b).

We note that in the large bias limit a quantum master equation can be derived without having to using the Born-Markov approximation [67]. Furthermore, the nondiagonal elements between states of different electron numbers become dynamically decoupled, without having to invoking additional assumptions, which largely extends the applicability of our results.

In the stationary limit when the counting time t is much longer than the time of tunneling through the system, the CGF is simply given by [68]

$$\mathcal{F}(\chi) = \lambda_0(\chi) t, \tag{8}$$

where $\lambda_0(\chi)$ is the unique eigenvalue of $\mathcal{L}(\chi)$ that satisfies $\lambda_0(\chi \to 0) \to 0$. However, as for the present system, an analytical solution is not available, one has to solve Eq. (7)

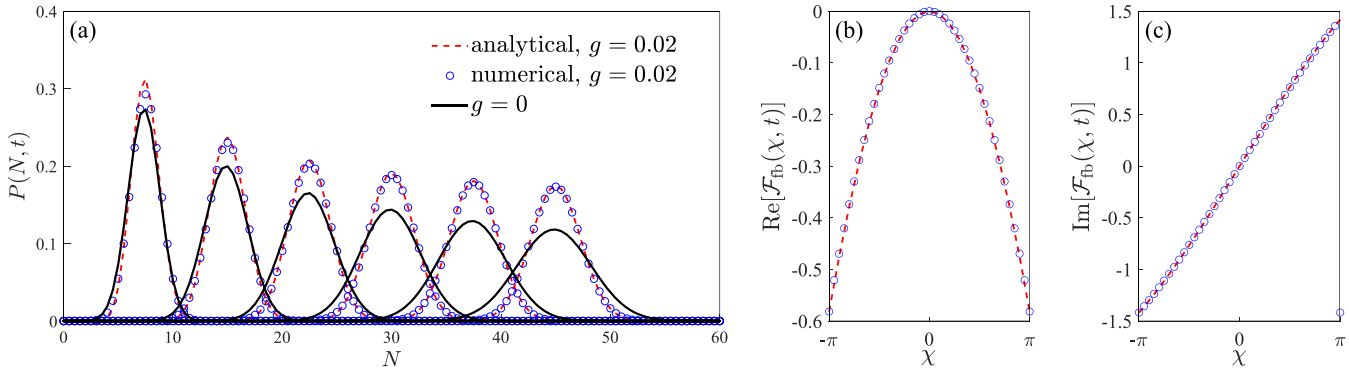

FIG. 2. (a) Feedback-controlled probability distributions for the number N of tunneled electrons at different times $t/\Gamma^{-1} = 30,\ 60,\ 90,\ 120,\ 150,$ and 180 under large bias using analytical (dashed curves) and numerical (circle) calculations. The results without feedback are shown by the solid curve for comparison. (b) Real part $\mathrm{Re}[\mathcal{F}_{\mathrm{fb}}(\chi,t)]$ and (c) imaginary part $\mathrm{Im}[\mathcal{F}_{\mathrm{fb}}(\chi,t)]$ of the CGF under feedback control using analytical (dashed curve) and numerical (circle) calculations at time $t = 2\Gamma^{-1}$. The other plotting parameters are $\Gamma_{\mathrm{L}} = \Gamma_{\mathrm{R}} = 2\Omega$, $\Delta E = 0$, and $\gamma_d = 0$. We use $\Gamma = \frac{1}{2}(\Gamma_{\mathrm{L}} + \Gamma_{\mathrm{R}})$ as unit of energy, the stationary current as the target current, and homogeneous feedback ($g_{\mathrm{L}} = g_{\mathrm{R}} = g_\Omega = g$).

numerically. At time $t = 0$, when the counting starts, one has $\rho^{(N)}(t = 0) = \rho_{\mathrm{st}}\delta_{N,0}$, thus it has to be solved with the initial condition $\rho(\chi, t = 0) = \rho_{\mathrm{st}}$, where ρ_{st} is the stationary reduced density matrix obtained from the unconditional quantum master equation. With the solution of Eq. (7), one readily obtains $\mathcal{F}(\chi,t) = -\ln\{\mathrm{Tr}\rho(\chi,t)\}$, and all cumulants can be obtained numerically. In particular, the probability distribution for transferred electrons can be evaluated via

$$P(N,t) = \int_0^{2\pi} \frac{d\chi}{2\pi} e^{-iN\chi} e^{\mathcal{F}(\chi,t)}. \tag{9}$$

In Fig. 2, the solid curves show the numerical probability distributions $P(N,t)$ for the number of tunneled electrons through the DQD for a large bias voltage $V = 50\Gamma$ at different times $t/\Gamma^{-1} = 30,\ 60,\ 90,\ 120,\ 150,$ and 180. The average of the distribution, which corresponds to the average number of tunneled electrons, moves constantly with increasing time. Furthermore, the width of the probability distribution, which characterizes the shot noise, grows with time. The spreading of the distribution occurs even at equilibrium (bias $V = 0$), as shown by the solid curves in Figs. 7(a)–7(d), where the net current is zero but the width of the distribution still increases with time. It is thus of essential importance to introduce a closed-loop feedback control and use an appropriate approach to investigate how to "freeze" the probability distribution in order to obtain a stabilized low noise current.

III. FEEDBACK SCHEME AND NUMERICAL APPROACH

A. Feedback scheme

The basic principle of the closed-loop feedback control scheme of transport through the DQD is schematically shown in Fig. 1, where the number of tunneled electrons N detected by the QPC is compared with the target number of electrons $I_{\mathrm{g}}t$. The discrepancy is fed back into the DQD transport device via modulating the gate voltages V_{GL}, V_{GR}, and $V_{\mathrm{G}\Omega}$, which amounts to a change of the tunneling rates through the corresponding barriers in the DQD.

First, we introduce $q_N(t)$ to describe the discrepancy between the target and detected number of tunneled electrons

$$q_N(t) = I_{\mathrm{g}}t - N, \tag{10}$$

where I_{g} is the target current and N is the number of detected charges. This discrepancy $q_N(t)$ can be used to determine whether the transport process need to be speed up or slowed down. This is achieved by adjusting the voltage of V_{GL}, V_{GR}, and $V_{\mathrm{G}\Omega}$ as shown in Fig. 1. It effectively corresponds to a modulation of the tunneling rates, i.e., $\Gamma_{\mathrm{L}} \to \eta_{\mathrm{L}}[q_N(t)]\Gamma_{\mathrm{L}}$, $\Gamma_{\mathrm{R}} \to \eta_{\mathrm{R}}[q_N(t)]\Gamma_{\mathrm{R}}$. Different from the feedback control of a single QD where only a modulation of Γ_{L} and Γ_{R} is possible, the DQD device offers the opportunity to feedback control the interdot tunnel coupling via $\Omega \to \eta_\Omega[q_N(t)]\Omega$. Note, for more complicated systems, it is also possible to introduce other feedback parameters as long as they are controllable.

A possible feedback scheme is to use the exponential protocol [69] $\eta_\ell[q_N(t)] = e^{g_\ell \cdot q_N(t)} = \exp\{g_\ell(I_{\mathrm{g}}t - N)\}$, where g_ℓ is a dimensionless feedback parameter. It ensures the positiviy of modulated tunneling rates. To be consitent with the experiment [27], hereafter we consider weak feedback ($g_\ell \ll 1$) such that the exponential feedback reduces to a simple liner feedback:

$$\eta_\ell[q_N(t)] = 1 + g_\ell(I_{\mathrm{g}}t - N), \quad \ell \in \{\mathrm{L}, \mathrm{R}, \Omega\}. \tag{11}$$

In the following calculations, we always choose g_ℓ to be small to guarantee the positivity of the modulated tunneling rates.

Under feedback, the χ-dependent master equation in Eq. (7) is transformed to

$$\dot{\varrho}(\chi,t) = \tilde{\mathcal{L}}(\chi,t)\varrho(\chi,t), \tag{12a}$$

where $\varrho(\chi,t)$ is the χ-dependent reduced density matrix under closed-loop feedback control, and $\tilde{\mathcal{L}}(\chi,t)$, the

counterpart of $\mathcal{L}(\chi)$ under feedback, is given by

$$\tilde{\mathcal{L}}(\chi,t)=\begin{pmatrix} -\sum\limits_{\ell=\mathrm{L,R}}\tilde{\eta}_\ell\Gamma_\ell^+ & \tilde{\eta}_\mathrm{L}\Gamma_\mathrm{L}^- & e^{i\chi}\tilde{\eta}_\mathrm{R}\Gamma_\mathrm{R}^- & 0 & 0 & 0\\ \tilde{\eta}_\mathrm{L}\Gamma_\mathrm{L}^+ & -\tilde{\eta}_\mathrm{L}\Gamma_\mathrm{L}^- - \tilde{\eta}_\mathrm{R}\tilde{\Gamma}_\mathrm{R}^+ & 0 & e^{i\chi}\tilde{\eta}_\mathrm{R}\tilde{\Gamma}_\mathrm{R}^- & 0 & 2\tilde{\eta}_\Omega\Omega\\ e^{-i\chi}\tilde{\eta}_\mathrm{R}\Gamma_\mathrm{R}^+ & 0 & -\tilde{\eta}_\mathrm{R}\Gamma_\mathrm{R}^- - \tilde{\eta}_\mathrm{L}\tilde{\Gamma}_\mathrm{L}^+ & \tilde{\eta}_\mathrm{L}\tilde{\Gamma}_\mathrm{L}^- & 0 & -2\tilde{\eta}_\Omega\Omega\\ 0 & e^{-i\chi}\tilde{\eta}_\mathrm{R}\tilde{\Gamma}_\mathrm{R}^+ & \tilde{\eta}_\mathrm{L}\tilde{\Gamma}_\mathrm{L}^+ & -\sum\limits_{\ell=\mathrm{L,R}}\tilde{\eta}_\ell\tilde{\Gamma}_\ell^- & 0 & 0\\ 0 & 0 & 0 & 0 & -\Gamma_d-\gamma_d & -\Delta E\\ 0 & -\tilde{\eta}_\Omega\Omega & \tilde{\eta}_\Omega\Omega & 0 & \Delta E & -\Gamma_d-\gamma_d \end{pmatrix}. \tag{12b}$$

Here $\Gamma_d=\frac{1}{2}\sum_{\ell=\mathrm{L,R}}\tilde{\eta}_\ell(\Gamma_\ell^-+\tilde{\Gamma}_\ell^+)$ and

$$\tilde{\eta}_\ell\equiv\tilde{\eta}_\ell[q_\chi(t)]=1+g_\ell(I_\mathrm{g}t-\partial_{i\chi}) \tag{13}$$

is the counterpart of Eq. (11) in χ space. By acting on the density matrix, the partial derivative $\partial_{i\chi}$ evaluates the number of already tunneled electrons. Our formalism allows thus to describe the number-based feedback action solely in terms of the reduced density matrix.

Now the central task is to utilize Eq. (12) to find the χ-dependent reduced density matrix under feedback $\varrho(\chi,t)$ such that one can obtain the CGF $\mathcal{F}_\mathrm{fb}(\chi,t)=\ln[\mathrm{tr}\{\varrho(\chi,t)\}]$. The cumulants under feedback can be obtained by taking partial derivatives of $\mathcal{F}_\mathrm{fb}(\chi,t)$ with respect to the counting field. However, Eq. (12) cannot be as easily solved as Eq. (7), which is an ordinary first-order differential equation in time. As inferred from Eq. (13), Eq. (12) is a set of partial differential equations of both χ and t.

For very simply systems, such as a tunneling junction or a single QD system with symmetric tunnel couplings ($\Gamma_\mathrm{L}=\Gamma_\mathrm{R}$) and homogeneous feedback ($\tilde{\eta}_\mathrm{L}=\tilde{\eta}_\mathrm{R}=\tilde{\eta}$), $\tilde{\mathcal{L}}(\chi,t)$ reduces to $\tilde{\mathcal{L}}(\chi,t)\to\mathcal{L}(\chi)\tilde{\eta}$. In the stationary limit, $\mathcal{L}(\chi)$ can be further replaced by its minimal eigenvalues in Eq. (8), and the feedback master Eq. (12) greatly simplifies to

$$\dot{\varrho}(\chi,t)=\lambda_0(\chi)\tilde{\eta}[q_\chi(t)]\varrho(\chi,t). \tag{14}$$

It is only in this case that one may use the method of characteristics to find an anlytical result for $\varrho(\chi,t)$ [24–26].

This is, however, not possible for a DQD transport device. Due to the presence of level mismatch ΔE and measurement-induced dephasing γ_d, $\tilde{\mathcal{L}}(\chi,t)$ in Eq. (12b) cannot be reduced to $\mathcal{L}(\chi)\tilde{\eta}$ even for the special case $\Gamma_\mathrm{L}=\Gamma_\mathrm{R}=\Omega$ and $\tilde{\eta}_\mathrm{L}=\tilde{\eta}_\mathrm{R}=\tilde{\eta}_\Omega=\tilde{\eta}$. Even if $\tilde{\mathcal{L}}(\chi,t)\to\mathcal{L}(\chi)\tilde{\eta}$ under very special conditions, normally it is not possible to get the minimal eigenvalue of $\mathcal{L}(\chi)$ in Eq. (7b) analytically. Furthermore, even though the minimal eigenvalue is obtained and one gets an equation similar to Eq. (14), the complicated form of $\lambda_0(\chi)$ may not allow an analytical solution of $\varrho(\chi,t)$. It is therefore necessary to use an appropriate approach for evaluating the transport characteristics under closed-loop feedback control.

B. Auxiliary density matrix approach

Now we are in a position to introduce an auxiliary density matrix approach to account for the feedback-controlled transport characteristics. To this end, we introduce the kth tier auxiliary reduced density matrix

$$\varrho_{[k]}(\chi,t)=\partial_{i\chi}^k\varrho(\chi,t)\quad(k\geqslant 0) \tag{15}$$

and decompose $\tilde{\mathcal{L}}(\chi,t)$ in the two parts:

$$\tilde{\mathcal{L}}(\chi,t)=\boldsymbol{\alpha}(\chi,t)+\boldsymbol{\beta}(\chi)\partial_{i\chi}, \tag{16}$$

where the partial derivative with respective to the counting field is singled out on purpose. Thereby,

$$\boldsymbol{\alpha}(\chi,t)=\tilde{\mathcal{L}}(\chi,t)|_{\tilde{\eta}_\ell\to 1+g_\ell I_\mathrm{g}t}, \tag{17a}$$

$$\boldsymbol{\beta}(\chi)\partial_{i\chi}=\tilde{\mathcal{L}}(\chi,t)-\boldsymbol{\alpha}, \tag{17b}$$

where $\boldsymbol{\alpha}(\chi,t)$ depends on both χ and t, while $\boldsymbol{\beta}(\chi)$ only depends on the counting filed χ. Taking partial derivatives with respect to the counting field $\partial_{i\chi}$ on Eq. (12) k times, we obtain the k differential equations

$$\dot{\varrho}_{[0]}=\boldsymbol{\alpha}\varrho_{[0]}+\boldsymbol{\beta}\varrho_{[1]}, \tag{18a}$$

$$\dot{\varrho}_{[1]}=(\partial_{i\chi}\boldsymbol{\alpha})\varrho_{[0]}+(\boldsymbol{\alpha}+\partial_{i\chi}\boldsymbol{\beta})\varrho_{[1]}+\boldsymbol{\beta}\varrho_{[2]}, \tag{18b}$$

$$\cdots=\cdots \tag{18c}$$

$$\dot{\varrho}_{[k]}=\big(\partial_{i\chi}^k\boldsymbol{\alpha}\big)\varrho_{[0]}+\big(k\partial_{i\chi}^{k-1}\boldsymbol{\alpha}+\partial_{i\chi}^k\boldsymbol{\beta}\big)\varrho_{[1]}+\cdots+\boldsymbol{\beta}\varrho_{[k+1]}. \tag{18d}$$

It results in a set of hierarchically coupled differential equations, where for an arbitrary k ($k\geqslant 1$), $\varrho_{[k]}$ is coupled to all the tiers from $\varrho_{[0]}$ to $\varrho_{[k+1]}$. By introducing a supervector $\boldsymbol{\mu}=\{\varrho_{[0]},\varrho_{[1]},\cdots,\varrho_{[k]}\}^\mathrm{T}$, Eq. (18) can be rewritten as

$$\dot{\boldsymbol{\mu}}(\chi,t)=\mathcal{Z}(\chi,t)\boldsymbol{\mu}(\chi,t), \tag{19a}$$

where the supermatrix $\mathcal{Z}(\chi,t)$ is given by

$$\mathcal{Z}(\chi,t)=\begin{pmatrix}\boldsymbol{\alpha}(\chi,t) & \boldsymbol{\beta}(\chi) & 0 & 0 & \cdots & 0 & 0\\ \partial_{i\chi}\boldsymbol{\alpha}(\chi,t) & \boldsymbol{\alpha}(\chi,t)+\partial_{i\chi}\boldsymbol{\beta}(\chi) & \boldsymbol{\beta}(\chi) & 0 & \cdots & 0 & 0\\ \partial_{i\chi}^2\boldsymbol{\alpha}(\chi,t) & 2\partial_{i\chi}\boldsymbol{\alpha}(\chi,t)+\partial_{i\chi}^2\boldsymbol{\beta}(\chi) & \boldsymbol{\alpha}(\chi,t)+2\partial_{i\chi}\boldsymbol{\beta}(\chi) & \boldsymbol{\beta}(\chi) & \cdots & 0 & 0\\ \vdots & \vdots & \vdots & \vdots & \ddots & \vdots & \vdots\\ \partial_{i\chi}^k\boldsymbol{\alpha}(\chi,t) & k\partial_{i\chi}^{k-1}\boldsymbol{\alpha}(\chi,t)+\partial_{i\chi}^k\boldsymbol{\beta}(\chi) & \cdots & \cdots & \cdots & \boldsymbol{\alpha}(\chi,t)+k\partial_{i\chi}\boldsymbol{\beta}(\chi) & \boldsymbol{\beta}(\chi)\end{pmatrix}. \tag{19b}$$

It should be noted that each element in Eq. (19b) is itself a matrix in the Hilbert space of the reduced system given by Eqs. (12b) and (17). At time $t=0$ when the counting starts, one has $\varrho^{(N)}(t=0)=\rho_{\rm st}\delta_{N,0}$, such that $\varrho_{[0]}(\chi,t=0)=\varrho(\chi,t=0)=\rho_{\rm st}$ and $\varrho_{[k]}(\chi,t=0)=\partial_{i\chi}^k\varrho(\chi,t=0)=0$ for $k\geqslant 1$. Equation (19) thus should be solved with the initial condition $\boldsymbol{\mu}(t=0)=\{\rho_{\rm st},0,\cdots,0\}^{\rm T}$, where $\rho_{\rm st}=\rho(t\to\infty)$ is the stationary reduced density matrix.

We mention that auxiliary density matrices have been used to evaluate the cumulants in mesoscopic transport described by the hierarchy equation of motions, see, for instance, Ref. [57]. There, the kth tier auxiliary density matrix is only coupled to the lower tier density matrices. Therefore they form a closed set of equations of motion. In the presence of feedback control, however, the kth auxiliary density matrix is not only coupled to the lower tier matrices, but also to a higher $(k+1)$th tier matrix. One thus has to solve Eq. (19) up to a sufficient large tier M ($M\gg k$) in order to obtain the accurate kth cumulant. In our practical numerical calculation, the truncation is made in the following way: We solve Eq. (19) up to the Mth tier provided that the difference of the kth cumulants calculated up to the Mth and $(M+1)$th tiers (δC_k) is negligibly small.

By numerically solving Eq. (19), one obtains the CGF under feedback control $\mathcal{F}_{\rm fb}(\chi,t)$

$$e^{\mathcal{F}_{\rm fb}(\chi,t)}={\rm tr}\{\varrho_{[0]}(\chi,t)\}={\rm tr}\{\varrho(\chi,t)\}. \tag{20}$$

The corresponding probability distribution is simply obtained via

$$P(N,t)=\int_0^{2\pi}\frac{d\chi}{2\pi}e^{-iN\chi}e^{\mathcal{F}_{\rm fb}(\chi,t)}. \tag{21}$$

In Figs. 2(b) and 2(c), we show, respectively, the real and imaginary parts of the numerically obtained feedback CGF $\mathcal{F}_{\rm fb}(\chi,t)$ evaluated up to 100 tiers ($M=100$) for the case of $\Gamma_{\rm L}=\Gamma_{\rm R}=2\Omega$, $U=0$, and bias $V/\Gamma=50$, cf. the circles.

Due to its construction, the solution of Eq. (19) yields directly the kth ($k\geqslant 1$) moment under feedback control

$$\begin{aligned}v_k(t)&={\rm tr}\{\varrho_{[k]}(\chi,t)\}|_{\chi\to 0}=\partial_{i\chi}^k{\rm tr}\{\rho(\chi,t)\}|_{\chi\to 0}\\&=\partial_{i\chi}^k e^{\mathcal{F}_{\rm fb}(\chi,t)}|_{\chi\to 0}.\end{aligned} \tag{22}$$

Utilizing the relation between cumulants and moments [70], one can readily calculate arbitrary cumulants. For instance, the first cumulant is the same as the first moment

$$C_1(t)=v_1(t), \tag{23}$$

and the second cumulant is given by

$$C_2(t)=v_2(t)-v_1^2(t). \tag{24}$$

Higher order cumulants can be obtained in a similar manner.

C. Delayed feedback

So far, we have considered instantaneous feedback, i.e., the control operations are performed directly after the measurement. Yet, realistically, time delay in the feedback control has to be taken into account. Now we are in a position to discuss the influence of a delayed feedback, which can be modeled by introducing a delay function $\xi(t')=\frac{1}{\tau}e^{-\frac{t'}{\tau}}$ to the tunneling rates. For simplicity, we assume homogeneous feedback ($g_{\rm L}=g_{\rm R}=g_\Omega=g$) and the resonance condition ($\Delta E=0$). The QME under delayed feedback then reads

$$\begin{aligned}\dot\rho(\chi,t)=\mathcal{L}(\chi)\int_0^t dt'\xi(t')[1+g(I_{\rm g}(t-t')-\partial_{i\chi})]\\ \times\ \rho(\chi,t-t'),\end{aligned} \tag{25}$$

where $\mathcal{L}(\chi)$ is given in Eq. (7b). In the long-time limit, it reduces to

$$\begin{aligned}\dot v_0(\chi,t)=\lambda_0(\chi)\int_0^t dt'\xi(t')[1+g(I_{\rm g}(t-t')-\partial_{i\chi})]\\ \times\ v_0(\chi,t-t'),\end{aligned} \tag{26}$$

where $v_0(\chi,t)={\rm tr}[\rho(\chi,t)]$ and $\lambda_0(\chi)$ is the minimal eigenvalue of $\mathcal{L}(\chi)$ in the absence of feedback. Although an explicit expression of $\lambda_0(\chi)$ may not be obtained, it is always possible to write $\lambda_0(\chi)=\langle\langle I\rangle\rangle\chi+\frac{1}{2!}\langle\langle I^2\rangle\rangle\chi^2+\cdots$, where $\langle\langle I\rangle\rangle$ and $\langle\langle I^2\rangle\rangle$ are, respectively, the stationary current and shot noise in the absence of feedback.

Upon transformation into the Laplace space, $\tilde v_0(\chi,z)=\int_0^\infty dt e^{-zt}v_0(\chi,t)$, Eq. (26) becomes

$$z\tilde v_0(\chi,z)-1=\lambda_0(\chi)\tilde\xi(z)(1-gI_{\rm g}\partial_z-g\partial_{i\chi})\tilde v_0(\chi,z), \tag{27}$$

where we have used the initial condition $v_0(\chi,t=0)=1$, and $\tilde\xi(z)=(1+z\tau)^{-1}$ is the delay function in the Laplace domain. For $\chi=0$, $\lambda_0(\chi=0)=0$, the above equation yields $\tilde v_0(0,z)=1/z$. Taking the first partial derivative of Eq. (27) with respective to $i\chi$ and let $\chi\to 0$, we obtain

$$\partial_{i\chi}\tilde v_0(\chi,z)|_{\chi\to 0}=\frac{z+gI_{\rm g}}{z+\tau z^2+g\langle\langle I\rangle\rangle}\frac{\langle\langle I\rangle\rangle}{z^2}. \tag{28}$$

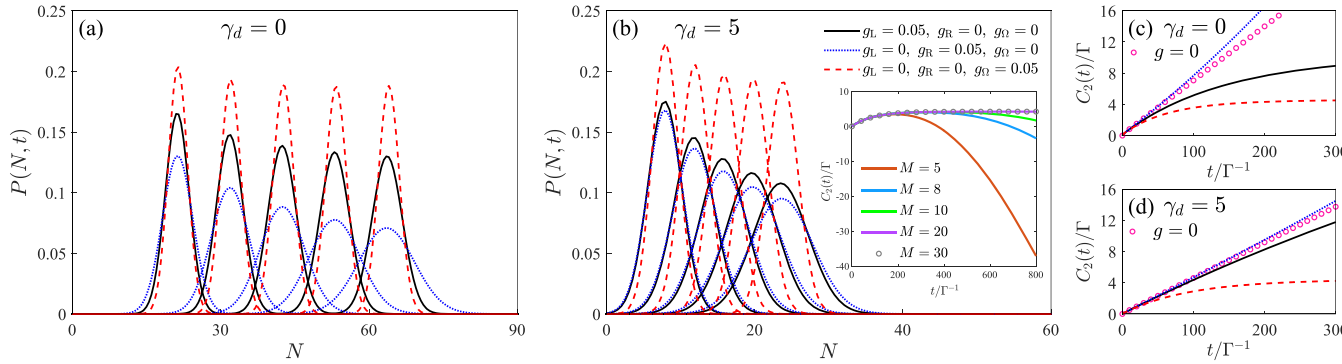

FIG. 3. Probability distributions for (a) $\gamma_d = 0$ and (b) $\gamma_d = 5\Gamma$ at times $t/\Gamma^{-1} = 120,\ 180,\ 240,\ 300,$ and 360. Each set of distributions is given only one of the three feedback parameters (g_L, g_R, and g_Ω) while the other two feedback parameters are zero. The corresponding second cumulants versus time are shown in (c) and (d), respectively, where the results without feedback ($g_L = g_R = g_\Omega = g = 0$) are also shown by the circles for comparison. The other plotting parameters are $\Gamma_L = 0.4\Gamma$, $\Gamma_R = 1.6\Gamma$, and $\Omega = 0.5\Gamma$, $\Delta E = 0.5\Gamma$, where $\Gamma = \frac{1}{2}(\Gamma_L + \Gamma_R)$ is set as unit of energy. We use the stationary current as the target current. (Inset) Second cumulant $C_2(t)$ obtained using various M to show the convergence with increasing tier number.

Applying the inverse Laplace transformation, one finds the first cumulant in the long-time limit becomes

$$C_{D1} = \partial_{i\chi} v_0(\chi, t)|_{\chi\to 0, t\to\infty} = I_g t. \tag{29}$$

It reveals that the probability distribution moves constantly with the target current, which is not affected by the time delay in feedback.

Analogously, taking the second partial derivative of Eq. (27) with respective to $i\chi$ and letting $\chi \to 0$, we obtain the second cumulant under delayed feedback in the long-time limit

$$\begin{aligned} C_{D2} &= \partial^2_{i\chi} v_0(\chi, t)|_{\chi\to 0, t\to\infty} - C^2_{D1}(t\to\infty) \\ &= \frac{I_g}{2g\langle\langle I\rangle\rangle}(F - 2I_g\tau), \end{aligned} \tag{30}$$

where $F = \frac{\langle\langle I^2\rangle\rangle}{\langle\langle I\rangle\rangle}$ is the usual Fano factor in the absence of feedback. It implies that the probability distribution can be frozen with a slightly modified but constant width.

Equation (30) seemingly suggests that the second cumulant can be negative for $I_g\langle\langle I\rangle\rangle < 0$, i.e., when the stationary current and the target current are not equally directed. While mathematically correct, this result must be discarded on physical grounds. Inspection of the equation of motion in Eq. (25) shows that feedback cannot reverse the direction of the current, but only amplify or deamplify it. Consequently, a negative I_g and positive $\langle\langle I\rangle\rangle$ will lead to negative transition rates in the Liovillian for long times according to Eq. (11). This will give rise to negative probabilities and, eventually, to a second cumulant, that is formally negative. This is apparently in contradiction to the weak feedback limit ($g_\ell \ll 1$) that guarrantees the positivity of the rates all the time. Likewise, a positive I_g and a negative $\langle\langle I\rangle\rangle$ will lead to diverging tunneling rates, that will be mathematically reflected in a negative second cumulant.

Intriguingly, a finite time delay $\tau > 0$ leads to a reduction of the fluctuations. The improvement can be explained as follows. Without time delay, the feedback action *overshoots* when trying to reach the target current. A finite time delay prevents this overshooting by slowing down the feedback action. For large enough τ, the second cumulant can become negative. In this case, the feedback action is so much delayed such that it cannot compensate the fluctuations. Similar to the case above, tunneling rates in the Louvillian will eventually become negative for increasing fluctuations. In this case, the solution Eq. (30) must be discarded on physical grounds.

IV. RESULTS AND DISCUSSION

A. Homogenous feedback

We are now in position to investigate feedback-controlled transport through a DQD device for various parameters. First, let us consider the special situation of $\Gamma_L = \Gamma_R = 2\Omega$, resonant levels $\Delta E = 0$, without QPC induced dephasing ($\gamma_d = 0$), homogeneous feedback $g_L = g_R = g_\Omega = g$, and large bias limit such that the Fermi functions can be approximated by either 1 or 0. It is only in this very special case that a simple minimal eigenvalue can be obtained $\lambda_0 = \Gamma(e^{i\frac{\chi}{4}} - 1)$, such that in the long-time limit, Eq. (12) reduces to

$$\dot{\varrho}(\chi, t) = \lambda_0(\chi)\{1 + g(I_g t - \partial_{i\chi})\}\varrho(\chi, t). \tag{31}$$

By using the method of characteristics, one arrives at the following CGF under feedback

$$\begin{aligned} \mathcal{F}_{fb}(\chi, t) =& \frac{4}{g}\{\mathrm{Li}_2[(1 - e^{-i\frac{\chi}{4}})e^{-g\frac{\Gamma}{4}t}] - \mathrm{Li}_2(1 - e^{-i\frac{\chi}{4}})\} \\ &+ iI_g t\chi + \frac{4}{g}\ln[e^{i\frac{\chi}{4}}(1 - e^{-g\frac{\Gamma}{4}t}) + e^{-g\frac{\Gamma}{4}t}], \end{aligned} \tag{32}$$

where $\mathrm{Li}_2(x)$ is the second-order polylogarithm function defined as $\mathrm{Li}_2(x) = \int_x^0 \frac{\ln(1-y)}{y} dy$. All the cumulants can be obtained by simply taking partial derivatives of $\mathcal{F}_{fb}(\chi, t)$ with respective to χ. For instance, the first cumulant yields $C_1 = I_g t$, and the second cumulant reads $C_2 = \frac{1}{8g}(1 - e^{-\frac{1}{2}g\Gamma t})$. Apparently, for finite feedback strength ($g > 0$), the second cumulant does not increase in time but converges to a constant. It implies that the charge probability distribution $P(N, t)$ does not spread out but freeze into a stationary distribution with a fixed width $C_2 = \frac{1}{8g}$ that moves constantly in time with a mean value $C_1 = I_g t$.

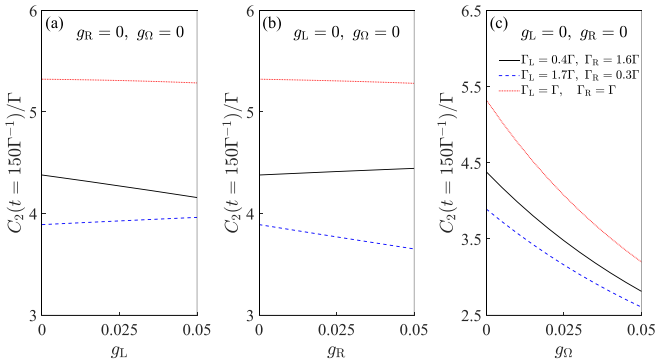

FIG. 4. (a) Second cumulant $C_2(t = 150\Gamma^{-1})$ vs g_L for $g_R = g_\Omega = 0$; (b) $C_2(t = 150\Gamma^{-1})$ vs g_R for $g_L = g_\Omega = 0$; and (c) $C_2(t = 150\Gamma^{-1})$ vs g_Ω for $g_L = g_R = 0$ under various tunnel couping configurations and large bias. The other plotting parameters are $\Delta E = 0.5\Gamma$ and $\gamma_d = 5\Gamma$, where $\Gamma = \frac{1}{2}(\Gamma_L + \Gamma_R)$ is set as unit of energy.

The analytical results of the probability distribution $P(N, t)$ and CGF $\mathcal{F}_{\rm fb}$ are plotted as dashed curves in Fig. 2, unambiguously demonstrating the striking agreement of numerical (circles) and analytical (dashed curves) results. Although these results are obtained under homogeneous feedback ($g_L = g_R = g_\Omega$) and very special conditions which may not correspond to real experimental parameters, it is still instructive to show the validity of the auxiliary density matrix approach under appropriate truncation.

B. Inhomogeneous feedback

Now we are in a position to consider the situation of inhomogeneous feedback. In this case, the numerical method is the sole option to investigate the effectiveness of feedback under different parameter configurations. Let us first consider the situation of a large bias voltage, i.e., $V \gg U, k_B T$ such that current flows through the DQD unidirectionally.

Figures 3(a) and 3(b) show, respectively, the probability distributions for $\gamma_d = 0$ and $\gamma_d = 5\Gamma$, with an arbitrary set of tunnel couplings ($\Gamma_L = 0.4\Gamma$, $\Gamma_R = 1.6\Gamma$, and $\Omega = 0.5\Gamma$). Each panel depicts a set of probability distributions for different times, at which only one of the three feedback parameters (g_L, g_R, and g_Ω) is finite, while the other two parameters are zero. For a fixed dephasing rate, the probability distributions move almost at the same pace as time increases under different feedback parameter configurations. However, finite dephasing due to the measurement by the QPC leads to localization of the electron in the DQD and thus suppresses the current. One thus observes that the probability distributions in Fig. 3(b) for $\gamma_d = 5\Gamma$ move slower than those for $\gamma_d = 0$ in Fig. 3(a).

Consider now the influence of feedback on noise properties. First, we have to confirm the number of minimum tiers M that has to be used in the numerical calculations. In the inset of Fig. 3(b), we plotted $C_2(t)$ for feedback parameter $g_L = g_R = 0$ and $g_\Omega = 0.5$ for different numbers of tiers. It is found that $M = 20$ is sufficient to obtain a stable $C_2(t)$. In the absence of feedback ($g_L = g_R = g_\Omega = g = 0$), the second-order cumulant $C_2(t)$ increases linearly with time, see the circles in Fig. 3. The presence of finite dephasing leads to an overall suppression of the shot noise. Strikingly, in the case of feedback with g_L=0, g_R=0.05, and $g_\Omega = 0$, $C_2(t)$ is even slightly larger than without feedback. This implies that the feedback control of Γ_R is not effective to suppress the noise. It is drastically different for g_L=0.05, g_R=0, and $g_\Omega = 0$. For $\gamma_d = 0$, the noise is apparently reduced by feedback via g_L, as shown by the solid curve in Fig. 3(c). However, in presence of finite dephasing, the feedback is inefficient and $C_2(t)$ grows almost linearly with time, cf. the solid curve in Fig. 3(d). Finally, it is found that g_Ω effectively freezes the probability distribution, regardless of the dephasing rates, see the dashed curves in Fig. 3(c) and 3(d).

For a detailed analysis, the second-order cumulant C_2 at a large time $t = 150\Gamma^{-1}$ is displayed as a function of feedback strength g_L, g_R, and g_Ω in Figs. 4(a)–4(c), respectively, for various tunnel couplings. Figure 4(a) shows that C_2 can be reduced by increasing g_L only for the case $\Gamma_L \ll \Gamma_R$ (cf. the solid curve), whereas it even increases slightly with g_L in the opposite case $\Gamma_L \gg \Gamma_R$ (see the dashed curve). Analogously, feedback via g_R is found to be effective in reducing noise only for $\Gamma_R \ll \Gamma_L$, as shown by the dashed curve in Fig. 4(b). Remarkably, g_Ω is always effective for various tunnel coupling asymmetries, as shown in Fig. 4(c). In particular, for $\Gamma_L = \Gamma_R$, the adjustment of neither g_L nor g_R is effective. Our findings thus reveal that g_Ω is the only effective feedback parameter to achieve the suppression of noise in this case.

Now we are in a position to investigate the effect of interdot Coulomb charging energy (U). For simplicity, we consider the strong interdot Coulomb blockade regime ($U \to \infty$), such that double occupation with one electron in each dot is not allowed. The Hilbert space is only spanned by the local dot states $|0\rangle$, $|\mathrm{L}\rangle$, and $|\mathrm{R}\rangle$, such that $\tilde{\mathcal{L}}(\chi, t)$ in Eq. (12b) reduces to a 5×5 matrix

$$\tilde{\mathcal{L}} = \begin{pmatrix} -\tilde{\eta}_L\Gamma_L & 0 & e^{i\chi}\tilde{\eta}_R\Gamma_R & 0 & 0 \\ \tilde{\eta}_L\Gamma_L & 0 & 0 & 0 & 2\tilde{\eta}_\Omega\Omega \\ 0 & 0 & -\tilde{\eta}_R\Gamma_R & 0 & -2\tilde{\eta}_\Omega\Omega \\ 0 & 0 & 0 & -\frac{\tilde{\eta}_R\Gamma_R}{2} - \gamma_d & -\Delta E \\ 0 & -\tilde{\eta}_\Omega\Omega & \tilde{\eta}_\Omega\Omega & \Delta E & -\frac{\tilde{\eta}_R\Gamma_R}{2} - \gamma_d \end{pmatrix}.$$

However, the reduction of the Hilbert space does not necessarily simplify the calculation. Rather, in the present situation, it is not possible to obtain an analytical minimal eigenvalue $\lambda_0(\chi)$. Therefore no analytical solution is available and the numerical method now is the only choice to investigate the feedback control.

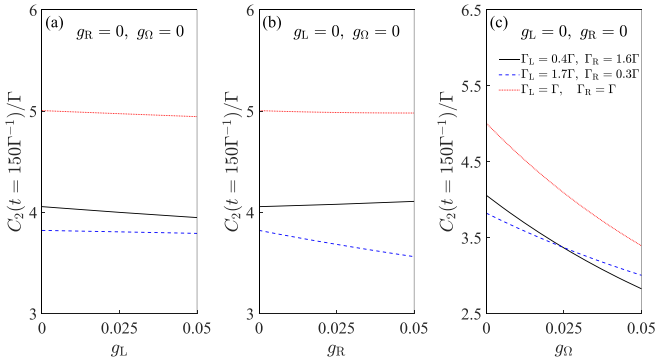

FIG. 5. (a) Second cumulant $C_2(t = 150\Gamma^{-1})$ vs g_L for $g_R = g_\Omega = 0$; (b) $C_2(t = 150\Gamma^{-1})$ vs g_R for $g_L = g_\Omega = 0$; and (c) $C_2(t = 150\Gamma^{-1})$ vs g_Ω for $g_L = g_R = 0$ for various tunnel couping asymmetry configurations in the limit of a large interdot Coulomb charging energy ($U \to \infty$). The other plotting parameters are the same as in Fig. 4.

The second cumulant C_2 at a large time ($t = 150\Gamma^{-1}$) with a strong interdot Coulomb charging energy ($U \to \infty$) is plotted as a function of g_L, g_R, and g_Ω in Figs. 5(a), 5(b) and 5(c), respectively, for various tunnel couplings. Analogous to those in Fig. 4, C_2 is plotted as a function of one of the three feedback parameters, while the other two feedback parameters are zero. The results are qualitatively similar to those in Fig. 5(a), with only the effectiveness of noise reduction quantitatively weakened slightly. Again, the feedback parameter g_Ω is the most effective feedback parameter for various tunnel coupling configurations.

It is worthwhile to mention that Eq. (19) allows to evaluate the cumulant up to an arbitrary order as long as one takes sufficiently large number of tiers. For example, in Fig. 6, we have plotted $C_8(t)$ for (a) $\gamma_d = 0$ and (b) $\gamma_d = 3\Gamma$, respectively, with homogeneous feedback ($g_L = g_R = g_\Omega = g$). A generalization to inhomogeneous feedback is straightforward. In the

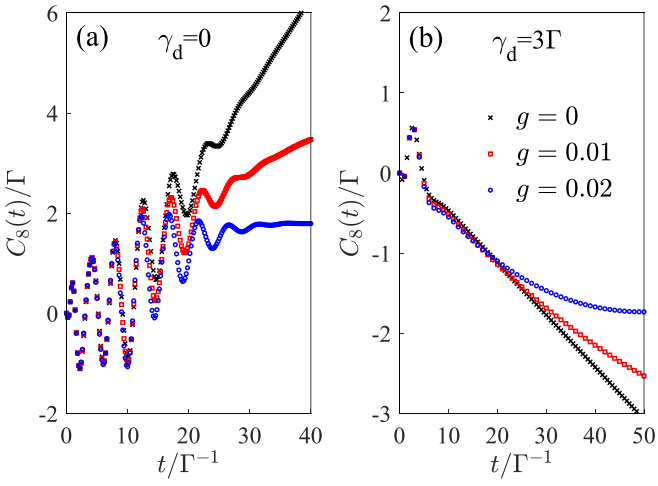

FIG. 6. $C_8(t)$ for (a) $\gamma_d = 0$ and (b) $\gamma_d = 3\Gamma$ under homogeneous feedback control with different feedback strengths. The other plotting parameters are $\Gamma_L = 0.4\Gamma$, $\Gamma_R = 1.6\Gamma$, $\Omega = 0.5\Gamma$, $k_B T = 10\Gamma$, $\Delta E = 0.5\Gamma$, and $\gamma_d = 5\Gamma$, where $\Gamma = \frac{1}{2}(\Gamma_L + \Gamma_R)$ is used as the unit of energy.

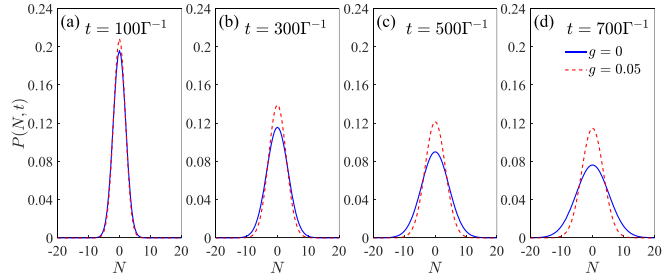

FIG. 7. Probability distributions in equilibrium ($V = 0$) at times (a) $t/\Gamma^{-1} = 100$, (b) 300, (c) 500, and (d) 700 without feedback (solid curves) and with homogeneous feedback for $g_L = g_R = g_\Omega = g = 0.05$ (dashed curves). The other plotting parameters are the same as those in Fig. 6.

limit of $\gamma_d = 0$ and $g = 0$ (absence of feedback), $C_8(t)$ undergoes some damped oscillations before it increases linearly with time, as shown by the crosses in Fig. 6(a). One observes a suppression of $C_8(t)$ in the presence of a small feedback strength $g = 0.01$. For $g = 0.02$, $C_8(t)$ is stabilized starting roughly from $t \gtrsim 35\Gamma^{-1}$. The situation becomes drastically different even for small dephasing rates, as shown in Fig. 6(b). Without feedback, $C_8(t)$ now is rapidly damped and then decreases with time. In the presence of a moderate feedback strength $g = 0.02$, $C_8(t)$ is stabilized from $t \gtrsim 50\Gamma^{-1}$.

C. Feedback of bidirectional transport

In comparison with a single QD, a unique advantage of a DQD transport system is that individual electrons tunneling in forward and reverse directions can be investigated in real time by using a QPC as a charge detector [56]. Measurement of the FCS for single QD devices is thus restricted to strong nonequilibrium conditions where transport is unidirectional [6–8,71,72]. Nevertheless, for the present DQD transport system, it is possible to detect bidirectional individual electron tunneling events via a nearby QPC and thus perform feedback control in the low bias regime.

Figure 7 shows the numerical probability distributions in equilibrium ($V = 0$) at different times. In this case, electrons tunnel in both forward and reverse directions with equal probabilities. The net current is zero and the probability distributions are thus centered at $N = 0$. The width of the probability distribution, however, spreads out as time increases in the absence of feedback, see the solid curves for $g = 0$. In the presence of finite feedback ($g = 0.05$), the probability distribution is clearly frozen for $t/\Gamma^{-1} > 500$, cf. the dashed curves. Our numerical results thus demonstrate that the measurement based feedback is capable of suppressing the noise of transport through a DQD even in equilibrium.

In Fig. 8(a), we have plotted the probability distributions for a small positive bias ($\mu_L = -\mu_R = 5\Gamma$). In this case, a small positive current flows through the DQD, regardless of the feedback strength, as shown in Fig. 8(c). We observe that the probability distributions under different feedback strengths move to the right at the same pace as time increases in Fig. 8(a). At a small time, however, there is quite a large probability to observe electron flowing in the reversed direction, see Fig. 8(a). In the opposite regime of

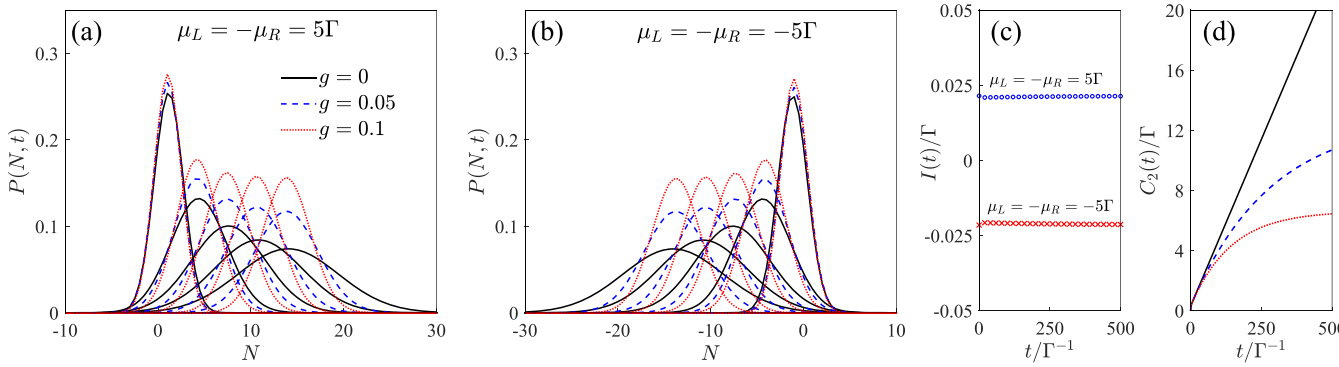

FIG. 8. Probability distributions for (a) a positive low bias ($\mu_{\rm L} = -\mu_{\rm R} = 5\Gamma$) and (b) a negative low bias ($\mu_{\rm L} = -\mu_{\rm R} = -5\Gamma$) at times $t/\Gamma^{-1} = 50$, 200, 350, 500, and 650; (c) the corresponding feedback currents $I(t)$; (d) second cumulant $C_2(t)$ for various feedback strengths. The other plotting parameters are the same as those in Fig. 6.

a small negative bias ($\mu_{\rm L} = -\mu_{\rm R} = -5\Gamma$), the probability distributions are displayed in Fig. 8(b). In this case, there is a negative current through the DQD, cf. Fig. 8(c). Therefore the probability distributions move to the reversed direction with time. Yet, one finds a finite probability for electrons traveling in the forward direction at small times, cf. Fig. 8(b). Essentially, the application of finite feedback is able to freeze the probability distribution as time increases, see for instance the dotted curves for $g = 0.1$. As the feedback strength $g_{\rm L} = g_{\rm R} = g_\Omega = g$ increases, the second cumulant rapidly stabilizes, see Fig. 8(d). These findings confirm that our feedback protocol works effectively in the regime of small bias where both forward and reverse tunneling coexists.

Let us now consider the situation when the target current $I_{\rm g}$ is different from the stationary current without feedback $\langle\langle I\rangle\rangle$. In Figs. 9(a) and 9(b), we have plotted, respectively, the feedback-controlled current $I(t)$ and the second cumulant $C_2(t)$ for three different cases of target currents: a larger target current than the stationary current ($I_g = 1.25\langle\langle I\rangle\rangle$), an equal target current to the stationary current ($I_g = \langle\langle I\rangle\rangle$), and a smaller target current than the stationary current ($I_g = 0.75\langle\langle I\rangle\rangle$). For simplicity, we assume homogeneous feedback ($g_{\rm L} = g_{\rm R} = g_\Omega = g = 0.1$). We clearly observe that in the long time, the feedback-controlled current always reaches the target current $I_{\rm g}$, rather than the stationary current without feedback $\langle\langle I\rangle\rangle$. Furthermore, our protocol for suppressing the noise still works even if $I_{\rm g}$ is different from $\langle\langle I\rangle\rangle$. The presence of a difference between $I_{\rm g}$ and $\langle\langle I\rangle\rangle$ only slightly modifies $C_2(t)$ quantitatively in the long-time limit.

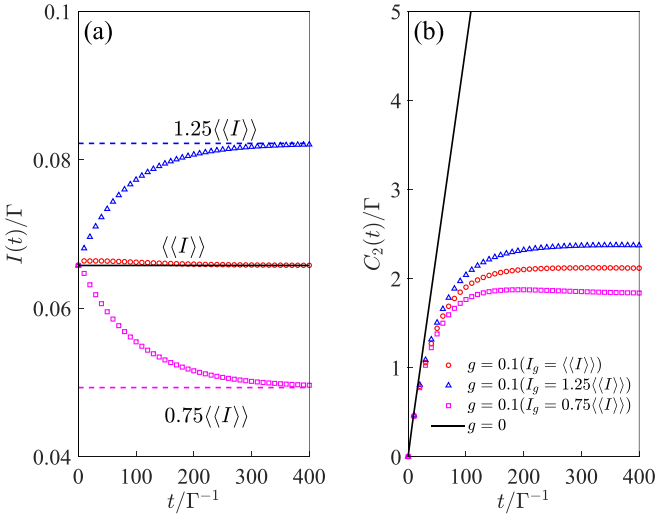

FIG. 9. (a) Feedback-controlled current $I(t)$ and (b) second cumulant $C_2(t)$ when the target current $I_{\rm g}$ is different from the stationary current without feedback $\langle\langle I\rangle\rangle$. We assume homogeneous feedback ($g_{\rm L} = g_{\rm R} = g_\Omega = g = 0.1$). The results in the absence of feedback ($g = 0$) are also shown by the solid curve for comparison. The other plotting parameters are the same as those in Fig. 6.

V. CONCLUSION

We have investigated the noise suppression of a double quantum dot transport system based on a closed-loop feedback control, where the information of the number of tunneled electrons detected by a nearby QPC is fed back into the device to stabilize the current. In order to characterize the counting statistics in the presence of feedback action, we developed an auxiliary density matrix approach motivated by the hierarchical expansion of the moment-generating function in the hierarchy equations of motion. This generic method has no restriction on the system structure and parameters and is able to evaluate the feedback current cumulants to an arbitrary order. Based on this approach, we demonstrate that the feedback scheme could effectively inhibit the noise in both low and high bias limits. In particular, it is revealed that the feedback control of the tunnel coupling between the two dots is the most effective under various tunnel coupling configurations. The presence of a strong interdot charging energy only slightly weakens the effect of feedback. The proposed feedback protocol for suppressing the noise even works if the target current is different from the stationary current. Finally, the influence of finite time delay has been analyzed, which reveals that feedback with time delays shorter than the time-scale of the inverse target current is still effective and only slightly modifies the frozen probability distribution. We anticipate that this work will facilitate low noise currents though coupled quantum dot systems via feedback control in near future experiments. We remark that by expanding

the generalized Liouvillian in Eq. (16) to higher orders in $\partial_{i\chi}$, the auxiliary density matrix method developed here can be even generalized to nonlinear feedback protocols, which will be investigated in a future work. Moreover, our methods can be also applied to control the photonic counting statistics of spontaneous [73–76] and stimulated [77] light emission.

ACKNOWLEDGMENTS

This work is supported by the National Natural Science Foundation of China (Grants No. 11774311 and No. 12005188) and education department of Zhejiang Province (No. 8). G.E. gratefully acknowledges financial support of the Guangdong Provincial Key Laboratory (Grant No. 2019B121203002).

[1] Y. M. Blanter and M. Büttiker, Phys. Rep. **336**, 1 (2000).
[2] Y. V. Nazarov (ed.), *Quantum Noise in Mesoscopic Physics* (Kluwer Academic, Dordrecht, 2003).
[3] M. Esposito, U. Harbola, and S. Mukamel, Rev. Mod. Phys. **81**, 1665 (2009).
[4] J. M. Elzerman, R. Hanson, L. H. W. van Beveren, B. Witkamp, L. M. K. Vandersypen, and L. P. Kouwenhoven, Nature (London) **430**, 431 (2004).
[5] M. Xiao, I. Martin, E. Yablonovitch, and H. Jiang, Nature (London) **430**, 435 (2004).
[6] E. V. Sukhorukov, A. N. Jordan, S. Gustavsson, R. Leturcq, T. Ihn, and K. Ensslin, Nat. Phys. **3**, 243 (2007).
[7] S. Gustavsson, R. Leturcq, B. Simovic, R. Schleser, T. Ihn, P. Studerus, K. Ensslin, D. C. Driscoll, and A. C. Gossard, Phys. Rev. Lett. **96**, 076605 (2006).
[8] S. Gustavsson, R. Leturcq, M. Studer, I. Shorubalko, T. Ihn, K. Ensslin, D. Driscoll, and A. Gossard, Surf. Sci. Rep. **64**, 191 (2009).
[9] A. Morello, J. J. Pla, F. A. Zwanenburg, K. W. Chan, K. Y. Tan, H. Huebl, M. Möttönen, C. D. Nugroho, C. Yang, J. A. van Donkelaar *et al.*, Nature (London) **467**, 687 (2010).
[10] M. Büttiker, Phys. Rev. Lett. **65**, 2901 (1990).
[11] L. Y. Chen and C. S. Ting, Phys. Rev. B **43**, 4534 (1991).
[12] J. Y. Luo, X.-Q. Li, and Y. J. Yan, Phys. Rev. B **76**, 085325 (2007).
[13] M. Henny, S. Oberholzer, C. Strunk, T. Heinzel, K. Ensslin, M. Holland, and C. Schönenberger, Science **284**, 296 (1999).
[14] W. D. Oliver, J. Kim, R. C. Liu, and Y. Yamamoto, Science **284**, 299 (1999).
[15] M. Misiorny, I. Weymann, and J. Barnaś, Phys. Rev. B **79**, 224420 (2009).
[16] I. Weymann, B. R. Bułka, and J. Barnaś, Phys. Rev. B **83**, 195302 (2011).
[17] Y. Okazaki, S. Sasaki, and K. Muraki, Phys. Rev. B **87**, 041302(R) (2013).
[18] D. Urban and J. König, Phys. Rev. B **79**, 165319 (2009).
[19] H.-F. Lu, J.-R. Zhang, T. Wu, X.-T. Zu, and H.-W. Zhang, J. Appl. Phys. **107**, 034314 (2010).
[20] R.-Q. Wang, L. Sheng, L.-B. Hu, B. G. Wang, and D. Y. Xing, Phys. Rev. B **84**, 115304 (2011).
[21] B. H. Wu and J. C. Cao, Phys. Rev. B **81**, 125326 (2010).
[22] J. Y. Luo, J. Hu, X. L. Lang, Y. Shen, X.-L. He, and H. J. Jiao, Phys. Lett. A **378**, 892 (2014).
[23] N. Ubbelohde, C. Fricke, F. Hohls, and R. J. Haug, Phys. Rev. B **88**, 041304(R) (2013).
[24] T. Brandes, Phys. Rev. Lett. **105**, 060602 (2010).
[25] C. Emary, *Feedback Control in Quantum Transport* (Springer International, Cham, 2016), pp. 275–287.
[26] T. Brandes, physica status solidi (b) **254**, 1600548 (2017).
[27] T. Wagner, P. Strasberg, J. C. Bayer, E. P. Rugeramigabo, T. Brandes, and R. J. Haug, Nat. Nanotechnol. **12**, 218 (2017).
[28] W. G. van der Wiel, S. D. Franceschi, J. M. Elzerman, T. Fujisawa, S. Tarucha, and L. P. Kouwenhoven, Rev. Mod. Phys. **75**, 1 (2002).
[29] W. H. Lim, H. Huebl, L. H. Willems van Beveren, S. Rubanov, P. G. Spizzirri, S. J. Angus, R. G. Clark, and A. S. Dzurak, Appl. Phys. Lett. **94**, 173502 (2009).
[30] D. P. Divincenzo, Science **309**, 2173 (2005).
[31] J. Stehlik, Y.-Y. Liu, C. Eichler, T. R. Hartke, X. Mi, M. J. Gullans, J. M. Taylor, and J. R. Petta, Phys. Rev. X **6**, 041027 (2016).
[32] A. J. Sigillito, M. J. Gullans, L. F. Edge, M. Borselli, and J. R. Petta, npj Quantum Inf. **5**, 110 (2019).
[33] W. Song, T. Du, H. Liu, R. Betzholz, and J. Cai, New J. Phys. **22**, 063029 (2020).
[34] K. Ono, D. G. Austing, Y. Tokura, and S. Tarucha, Science **297**, 1313 (2002).
[35] J. Fransson and M. Råsander, Phys. Rev. B **73**, 205333 (2006).
[36] J. Iñarrea, G. Platero, and A. H. MacDonald, Phys. Rev. B **76**, 085329 (2007).
[37] S. Gustavsson, M. Studer, R. Leturcq, T. Ihn, K. Ensslin, D. C. Driscoll, and A. C. Gossard, Phys. Rev. B **78**, 155309 (2008).
[38] K. Brown, M. Crisan, and I. Ţifrea, J. Phys.: Condens. Matter **21**, 215604 (2009).
[39] V. Meden and F. Marquardt, Phys. Rev. Lett. **96**, 146801 (2006).
[40] G. Kießlich, P. Samuelsson, A. Wacker, and E. Schöll, Phys. Rev. B **73**, 033312 (2006).
[41] H.-B. Xue, Ann. Phys. **339**, 208 (2013).
[42] J. N. Pedersen, B. Lassen, A. Wacker, and M. H. Hettler, Phys. Rev. B **75**, 235314 (2007).
[43] B. Wunsch, M. Braun, J. König, and D. Pfannkuche, Phys. Rev. B **72**, 205319 (2005).
[44] J. Y. Luo, H. J. Jiao, Y. Shen, G. Cen, X.-L. He, and C. Wang, J. Phys.: Condens. Matter **23**, 145301 (2011).
[45] P. Trocha, I. Weymann, and J. Barnaś, Phys. Rev. B **80**, 165333 (2009).
[46] P. Trocha, Phys. Rev. B **82**, 125323 (2010).
[47] G. Giavaras and Y. Tokura, Phys. Rev. B **100**, 195421 (2019).
[48] G.-M. Tang and J. Wang, Phys. Rev. B **90**, 195422 (2014).
[49] T. Gilad and S. A. Gurvitz, Phys. Rev. Lett. **97**, 116806 (2006).
[50] J. Y. Luo, Y. Shen, X.-L. He, X.-Q. Li, and Y. J. Yan, Phys. Lett. A **376**, 59 (2011).

[51] J. Y. Luo, H. J. Jiao, J. Hu, X.-L. He, X. L. Lang, and S.-K. Wang, Phys. Rev. B **92**, 045107 (2015).
[52] D. Y. Baines, T. Meunier, D. Mailly, A. D. Wieck, C. Bäuerle, L. Saminadayar, P. S. Cornaglia, G. Usaj, C. A. Balseiro, and D. Feinberg, Phys. Rev. B **85**, 195117 (2012).
[53] L. G. G. V. Dias da Silva, E. Vernek, K. Ingersent, N. Sandler, and S. E. Ulloa, Phys. Rev. B **87**, 205313 (2013).
[54] R. Härtle, G. Cohen, D. R. Reichman, and A. J. Millis, Phys. Rev. B **88**, 235426 (2013).
[55] R. Hussein and S. Kohler, Phys. Rev. B **89**, 205424 (2014).
[56] T. Fujisawa, T. Hayashi, R. Tomita, and Y. Hirayama, Science **312**, 1634 (2006).
[57] J. Cerrillo, M. Buser, and T. Brandes, Phys. Rev. B **94**, 214308 (2016).
[58] T. H. Stoof and Y. V. Nazarov, Phys. Rev. B **53**, 1050 (1996).
[59] B. L. Hazelzet, M. R. Wegewijs, T. H. Stoof, and Y. V. Nazarov, Phys. Rev. B **63**, 165313 (2001).
[60] G. Kießlich, E. Schöll, T. Brandes, F. Hohls, and R. J. Haug, Phys. Rev. Lett. **99**, 206602 (2007).
[61] T. Brandes, Phys. Rep. **408**, 315 (2005).
[62] R. Aguado and T. Brandes, Phys. Rev. Lett. **92**, 206601 (2004).
[63] S. A. Gurvitz, Phys. Rev. B **56**, 15215 (1997).
[64] J. Y. Luo, S.-K. Wang, X.-L. He, X.-Q. Li, and Y. J. Yan, J. Appl. Phys. **108**, 083720 (2010).
[65] S. A. Gurvitz and Y. S. Prager, Phys. Rev. B **53**, 15932 (1996).
[66] J. Y. Luo, Y. Yan, H. Wang, J. Hu, X.-L. He, and G. Schaller, Phys. Rev. B **101**, 125410 (2020).
[67] S. Gurvitz, Front. Phys. **12**, 120303 (2017).
[68] D. A. Bagrets and Y. V. Nazarov, Phys. Rev. B **67**, 085316 (2003).
[69] H. M. Wiseman and G. J. Milburn, *Quantum Measurement and Control*, 4th ed. (Cambridge University Press, Cambridge, 2010).
[70] L. Mandel and E. Wolf, *Optical Coherence and Quantum Optics* (Cambridge University Press, Cambridge, 1995).
[71] W. Lu, Z. Ji, L. Pfeiffer, K. W. West, and A. J. Rimberg, Nature (London) **423**, 422 (2003).
[72] J. Bylander, T. Duty, and P. Delsing, Nature (London) **434**, 361 (2005).
[73] R. J. Cook, Phys. Rev. A **23**, 1243 (1981).
[74] X. H. H. Zhang and H. U. Baranger, Phys. Rev. A **97**, 023813 (2018).
[75] F. Brange, P. Menczel, and C. Flindt, Phys. Rev. B **99**, 085418 (2019).
[76] K. N. Nesterov, I. V. Pechenezhskiy, and M. G. Vavilov, Phys. Rev. A **101**, 052321 (2020).
[77] G. Engelhardt, S. Choudhury, and W. V. Liu, arXiv:2207.08558.